Seeing Double: Transient Dips and Photometric Binarity in PTFO 8-8695

L. G. BOUMA[1] AND J. N. WINN[1]

[1] *Department of Astrophysical Sciences, Princeton University, 4 Ivy Lane, Princeton, NJ 08540, USA*

ABSTRACT

PTFO 8-8695b is a candidate hot Jupiter in the 7–10 million year old Orion-OB1a cluster. We inspected data from TESS and Gaia to clarify whether it is truly a planet. The Gaia data show that PTFO 8-8695 is a photometric binary with respect to members of its kinematic group. The TESS lightcurve shows that the dominant variability in this system is a sinusoid with a "long" period $P_\ell = 11.96$ hr, presumably caused by stellar rotation. Also present is a complex signal, previously identified as the planet candidate, that repeats with a "short" period $P_s = 10.74$ hr. The two signals beat every 4.48 days. Although there is a dip in the short-period signal, ground-based photometry from the past decade shows that the orbital phase of the dip seems to have instantaneously jumped, at least once, and perhaps twice. Planets do not "jump" in orbital phase. Given the evidence, we believe that PTFO 8-8695 is a binary M dwarf in which one star shows the long rotation signal, and the other star shows "transient dipping" that has been seen in a few other young weak-lined T Tauri stars. The origin of these transient dips is still undetermined, but our preferred explanation is eclipses of clouds of gas or dust at the Keplerian co-rotation radius.

1. INTRODUCTION

If PTFO 8-8695b were a planet, it would be exceptional. Transiting a sub-10 Myr old weak-lined T Tauri M dwarf in Orion, it would be the youngest hot Jupiter known (van Eyken et al. 2012). Its orbital period of only 10.7 hours would also give it the shortest period of any known hot Jupiter. With such a short period, it would almost certainly have filled its Roche lobe, and would be actively losing mass to its host star. Not only that, but the rapidly rotating host star would also be oblate and gravity darkened, and so the planet's orbit would likely precess into and out of transitability (Barnes et al. 2013; Ciardi et al. 2015; Kamiaka et al. 2015).

Other lines of evidence would imply further planetary "firsts" for this planet candidate. One first would be that its transits are about three times deeper in optical band-passes (*e.g., g*-band) than in the near-infrared (*e.g., z*-band) (Onitsuka et al. 2017; Tanimoto et al. 2020). A cloud-free hydrogen-dominated planetary atmosphere cannot explain such a wavelength dependence. The planet might therefore be surrounded by a dust cloud (Tanimoto et al. 2020).

Another first could be the direct detection of Hα emission from the planet itself (Johns-Krull et al. 2016). While the stellar chromosphere emits in Hα, it seems that there is an additional excess Hα emission that could be in phase with the planetary orbit. The average velocity width of the excess Hα emission is $87 \, \mathrm{km \, s^{-1}}$, and its equivalent width is 70-80% that of the stellar chromosphere (Johns-Krull et al. 2016). The proposed explanation is that outflowing mass from the planet may explain this excess emission as well (Johns-Krull et al. 2016).

There are perhaps a few challenges to the planetary interpretation (if these "features" are not already seen as such). They include that the planet does not seem to emit infrared radiation in occulation, at least anywhere near the expected amplitude (Yu et al. 2015). In addition, despite measurement attempts by multiple investigators, it does not seem to show the Rossiter effect at the amplitude expected given the rapid stellar rotation and large planet size (Yu et al. 2015; Ciardi et al. 2015). Finally, detailed modelling of the "precession + gravity darkening" transits has shown that the necessary degree of gravity darkening is too great, given the spectroscopically observed equatorial velocity (Howarth 2016). Additionally, as the gravity-darkened star precessed about its rotation axis, it would need to show photometric variability that has not been observed. While the planetary interpetation clearly faces challenges, alternative explanations do as

Corresponding author: L. G. Bouma
luke@astro.princeton.edu

well. High-latitude accretion hotspots might produce the observed Hα variability, and require fine-tuning produce dips of the approach duration. Furthermore, PTFO 8-8695 does not have an infrared (IR) excess associated with the presence of an inner disk (*e.g.*, Yu et al. 2015, Figure 18). Low-latitude starspots, hot or cold, struggle to produce the necessary dip durations.

Alternatively, between 0.1% and 1% of rapidly rotating low-mass stars in $\mathcal{O}(10)$ Myr old associations show narrow dips in phase with strong stellar rotation signals (Rebull et al. 2018). The dips can persist over months, but their depths often vary, and sometimes change immediately after stellar flares. The explanation proposed by Stauffer et al. (2017) and David et al. (2017) is that a circumstellar cloud of dust or gas might be orbiting near the Keplerian co-rotation radius. For this explanation to be viable for PTFO 8-8695, a clear determination of the stellar rotation period is necessary. To date this has not been possible (van Eyken et al. 2012; Koen 2015; Raetz et al. 2016).

We begin in Section 2 by describing newly available observations from TESS (Ricker et al. 2015) and Gaia (Gaia Collaboration et al. 2018). The TESS lightcurve shows two distinct signals, which we extract and analyze in Section 3. A long-period sinusoid repeats every 12.0 hours, and is probably stellar rotation. A short-period dip with an additional complex modulation repeats every 10.7 hours. Analyzing the Gaia data in Section 4, we show that relative to its kinematic group, PTFO 8-8695 is a photometric binary. We collect and discuss the puzzle pieces in Section 5. The orbital phase of the dip seems to have instantaneously changed over the past decade. In addition, a number of other young stars show lightcurve morphologies similar to the short-period signal. We therefore argue that PTFO 8-8695 is a binary M dwarf in which one star shows a rotation signal, and the other shows "transient dipping" caused by eclipses of material at the Keplerian co-rotation radius. Section 7 summarizes our main points.

2. THE DATA

2.1. *TESS Observations*

PTFO 8-8695 was observed by TESS with Camera 1, CCD 1, from December 15, 2018 to January 6, 2019, during the sixth sector of science operations (Ricker et al. 2015). The star was designated TIC 264461976 in the TESS Input Catalog (Stassun et al. 2018, 2019). The pixel data for an 11×11 array surrounding PTFO 8-8695 were averaged into 2-minute stacks by the onboard computer. Each 2048×2048 image from the CCD was also averaged into 30-minute stacks, and saved as a "full frame image" (FFI).

The 2-minute stacks for PTFO 8-8695 were reduced to lightcurves by the Science Processing Operations Center (SPOC) at NASA Ames (Jenkins et al. 2016). Our main analysis used the resulting Presearch Data Conditioning (PDC) lightcurve. The PDC lightcurve aperture used pixels chosen to maximize the SNR of the total flux of the target (Smith et al. 2017a). Non-astrophysical variability was removed through the methods discussed by Smith et al. (2017b).

As an independent check on the shorter cadence SPOC light-curve, we separately processed the 30-minute image stacks as part of the Cluster Difference Imaging Photometric Survey (CDIPS; Bouma et al. 2019). Our CDIPS lightcurve of choice used a circular aperture with radius 1 pixel.

To clean the data, we removed all points with non-zero quality flags (*e.g.*, Tenenbaum & Jenkins 2018). We also masked out the first and last 6 hours of each orbit, since there is often systematic red noise during those times. Both the CDIPS and PDC lightcurves showed a clear discontinuous "jump" in the last few days of orbit 20, which seemed likely to be an instrumental systematic. We correspondingly masked out times from BJD 2458488.3 until the end of the orbit. The PDC lightcurve initially had 15,678 points. The quality-flag cut removed 854 points; masking the orbit edges removed an additional 716; removing the final few days of orbit 20 removed an additional 1079. After cleaning, 83% of the initial flux measurements remained.

We normalized these points by dividing out the median flux. We opted to then subtract by unity to simplify subsequent interpretation. Many of these and subsequent processing steps were performed using `astrobase` (Bhatti et al. 2018).

2.2. *Gaia Observations*

#### 2.2.1. *Astrometry of PTFO 8-8695*

Between July 25, 2014 and May 23, 2016, Gaia measured about 300 billion centroid positions of 1.6 billion stars (Gaia Collaboration et al. 2016; Lindegren et al. 2018; Gaia Collaboration et al. 2018). In the Gaia second data release (DR2), these CCD observations were used to estimate positions, proper motions, and parallax for the brightest 1.3 billion stars, including PTFO 8-8695 (Lindegren et al. 2018). There were 121 "good" observations of PTFO 8-8695, that is observations that were not strongly down-weighted in its astrometric solution. PTFO 8-8695 was assigned a Gaia DR2 identifier of 3222255959210123904. It photometric brightness was measured using selected bands (G, Rp, and Bp) of the Gaia Radial Velocity Spectrometer (Cropper et al. 2018; Evans et al. 2018). We accessed the pipeline parameters for PTFO 8-8695 using the Gaia archive[1].

The majority of Gaia's derived parameters for PTFO 8-8695 agreed with expectation from former studies (Briceño et al. 2005; van Eyken et al. 2012). One novelty however was that Gaia DR2 detected a significant "astrometric excess", at a level of 10.3σ. We comment on the significance and interpretation of this excess in Section 4.

2.2.2. *Hierarchical Cluster Membership*

Gaia also provided astrometric parameters for tens of thousands of young stars in the Orion complex. The stellar populations in giant molecular cloud complexes are not monolithic; substructured groups are the norm (Briceño et al.

---

[1] gea.esac.esa.int/archive/
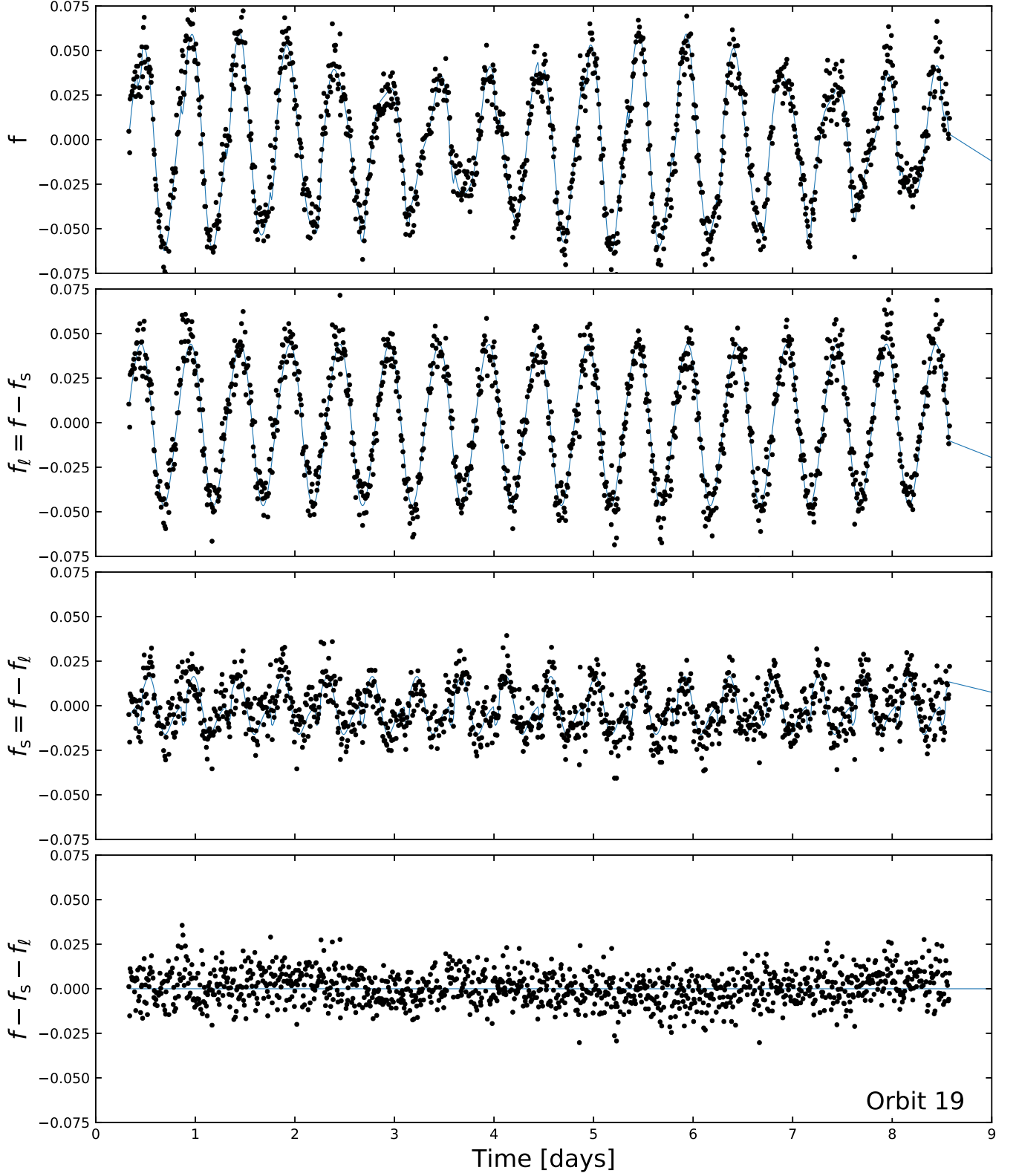
Figure 1. TESS lightcurve of PTFO 8-8695 (Sector 6, Orbit 19). *Top*: "Raw" `PDCSAP` mean-subtracted relative flux versus time. The beat period of 4.48 days is visible by eye. The preferred model plotted underneath the data includes 2 harmonics at the long period P_ℓ, plus 2 harmonics and a transit at the short period P_s. *Upper middle*: Long-period signal, equal to the raw signal minus the short-period signal. *Lower middle*: Short-period signal, equal to the raw signal minus the long-period signal. *Bottom*: residual. The data are binned from 2 to 10 minute cadence as a convenience for plotting and fitting.
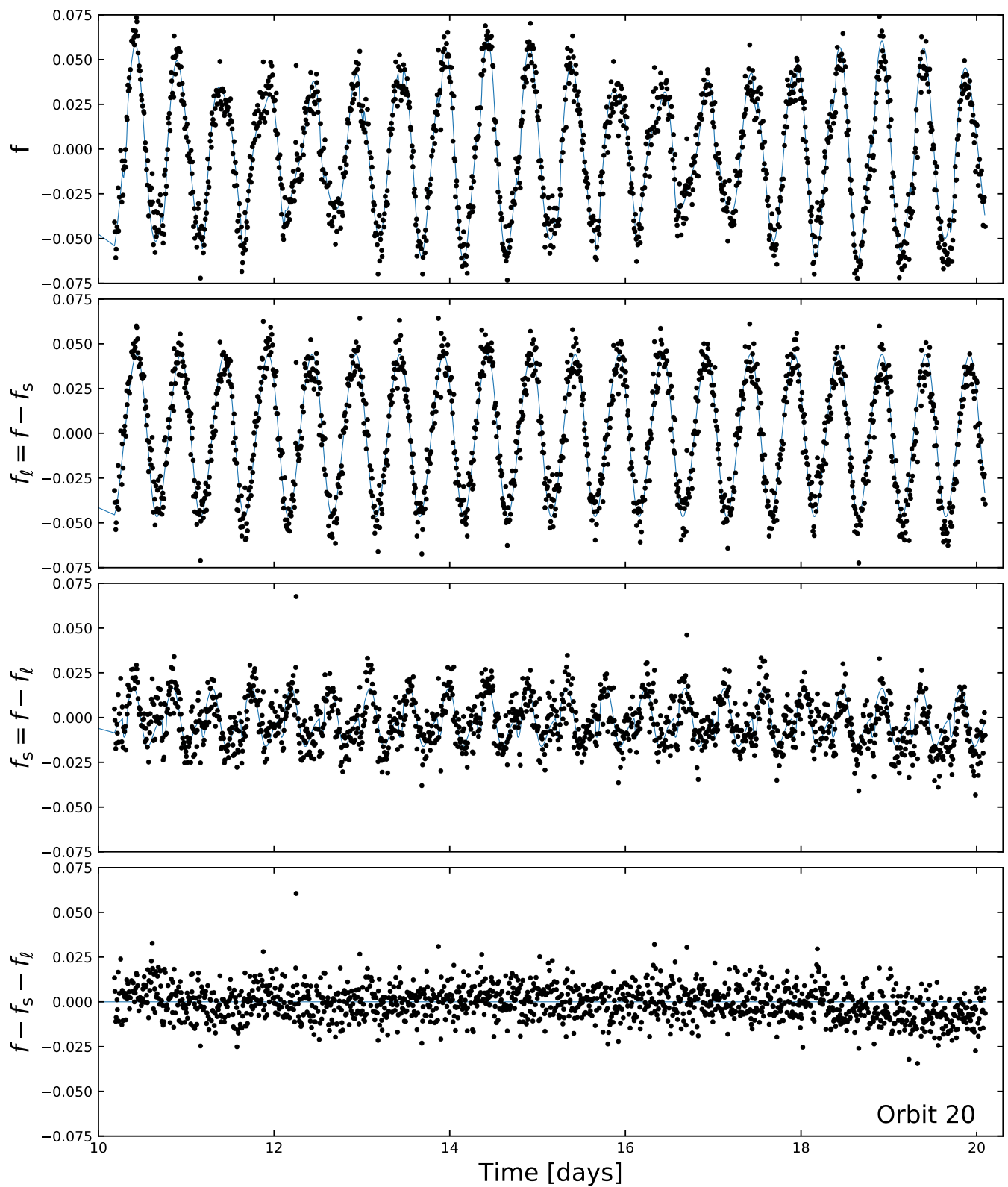
Figure 2. TESS lightcurve of PTFO 8-8695 (Sector 6, Orbit 20). Panels are as in Figure 1.

2007b). The Orion molecular cloud complex in particular has numerous subgroups, with ages spanning 0.5 to 15 Myr. For an incomplete sampling, see for instance Briceño et al. (2005); Jeffries et al. (2006); Briceño et al. (2007a); Kounkel et al. (2018) and Briceño et al. (2019).

PTFO 8-8695 was initially identified as a member of the Orion OB1a sub-association by Briceño et al. (2005) through combined photometry and spectroscopy. Later work by Briceño et al. (2007a) clarified that PTFO 8-8695 was in a kinematically distinct subgroup of Orion OB1a, named the "25 Ori" group after its brightest member. The 25 Ori group had an isochrone age of 7–10 Myr, and had a smaller disk fraction than younger nearby sub-associations (Hernández et al. 2007).

With the Gaia astrometry, it has become clear that 25 Ori itself has further subgroups (Kounkel et al. 2018; Briceño et al. 2019). In describing the cluster membership of PTFO 8-8695, we follow the notation and results of Kounkel et al. (2018). These authors combined astrometric data from Gaia DR2 with near-infrared spectra from APOGEE-2 (Gunn et al. 2006; Majewski et al. 2017; Blanton et al. 2017; Zasowski et al. 2017; Cottle et al. 2018). They performed a hierarchical clustering on the six dimensional position and velocity information to identify subgroups within the Orion complex. From smallest to largest, PTFO 8-8695 was identified as being a member of the following hierarchical subgroups:

$$25\,\text{Ori-1} \subset 25\,\text{Ori} \subset \text{Orion OB1a} \subset \text{Orion D}, \quad (1)$$

where from set-notation, '$\subset$' denotes "is a proper subset of". 25 Ori-1 is the largest subgroup of 25 Ori, with 149 identified members. Its mean age from its CMD was found to be 6.9 Myr, and from its HR diagram 8.5 Myr (Kounkel et al. 2018). Kounkel et al. (2018) identified seven other smaller groups in the Orion complex near the Be star 25 Ori. These groups received higher numbers, $e.g.$, 25 Ori-2 (Age$_{\text{CMD}}$ = 15.1 Myr; Age$_{\text{CMD}}$ = 12.9 Myr; see also Briceño et al. 2019).

These details concerning the group membership for one object may seem cumbersome to those accustomed to comparing "young cluster members" with "old field stars". Though all members of the Orion complex are indeed young relative to the field, these details are essential for assessing any evidence for photometric binarity in PTFO 8-8695, because of the degeneracy between stellar luminosity and age for pre-main-sequence stars. Having a clean sample of tightly spatially and kinematically associated reference stars minimizes contamination not just from the field, but from older and younger members of the Orion complex itself.

3. TESS ANALYSIS

3.1. *Inspection*

Our initial inspection of the TESS lightcurve, in both its 2-minute PDCSAP and 30-minute FFI forms, showed a strong sinusoidal beat signal (Figures 1 and 2, top panel).

As a precursor to more detailed analysis, we calculated generalized Lomb-Scargle periodograms using `astrobase` (Lomb 1976; Scargle 1982; VanderPlas & Ivezić 2015; Bhatti

et al. 2018). The two largest peaks in the Lomb-Scargle periodogram of the lightcurve were clearly separated at a "short" period $P_s \approx 0.448$ days and a "long" period $P_\ell \approx 0.499$ days. The P_ℓ peak had the greater power of the two. Smaller harmonics surrounding each of these two dominants peaks were also present.

The peak-to-peak lightcurve amplitude at maximum, when the two signals constructively interfere, is about 14%. At minimum, the peak-to-peak amplitude is about 6%. Assuming the signals are just two sinusoids, algebra tells us that the peak-to-peak amplitudes should therefore be 10% for the long-period signal, and 4% for the short-period signal. These order-of-magnitude numbers will turn out to be roughly correct.

Initial signal-processing experiments fitting out splines or sinusoids showed that after subtracting out the long-period signal, the short-period signal dominated the periodogram, and vice-versa. However it quickly became clear that it would be beneficial to simultaneously model the signals separately, in order to preserve the power at each frequency.

3.2. *Lightcurve Model*

We fitted the lightcurve as a linear combination of Fourier harmonics at the short and long periods, plus a transit at the short period. Symbolically, the total flux f is given as

$$f = f_s + f_\ell = f_{\text{transit,s}} + f_{\text{Fourier,s}} + f_{\text{Fourier,}\ell}, \quad (2)$$

where f_s is the relative flux at the short period, and f_ℓ is the flux at the long period. Writing out the Fourier terms,

$$f = f_{\text{transit,s}} + \sum_{n=1}^{N} A_n \sin(n\omega_s t) + \sum_{n=1}^{N} B_n \cos(n\omega_s t) \quad (3)$$

$$+ \sum_{m=1}^{M} A_m \sin(m[\omega_\ell t + \phi_\ell]) + \sum_{m=1}^{M} B_m \cos(m[\omega_\ell t + \phi_\ell]),$$

for N and M the total number of harmonics at the short and long periods, respectively, A_i and B_i the amplitudes for each harmonic term (potentially negative), and $\omega_i = 2\pi/P_i$ the angular frequency for i the short or long period index. We fixed the "phase-offset" for the short period signal to be zero, and let the reference time for the long period signal float by introducing ϕ_ℓ. Since we did not a priori know how many harmonics would be appropriate, we considered a number of different choices for N and M, and used the Bayesian information criterion to choose the appropriate model (Table 1).

As an example, one possible model could be a transit, plus $N = 2$ harmonics of sines and cosines at the short period, plus $M = 1$ harmonics at the long period. For this case the free parameters would be as follows. For the transit, we would fit for the impact parameter, the planet-to-star radius ratio, two quadratic limb darkening parameters, the planet orbital period (equal to the short period), the reference time for the transit, and the mean flux. There would be $2N = 4$ additional Fourier amplitudes at the short period, plus $2M = 2$ Fourier amplitudes at the long period, and well as the long period
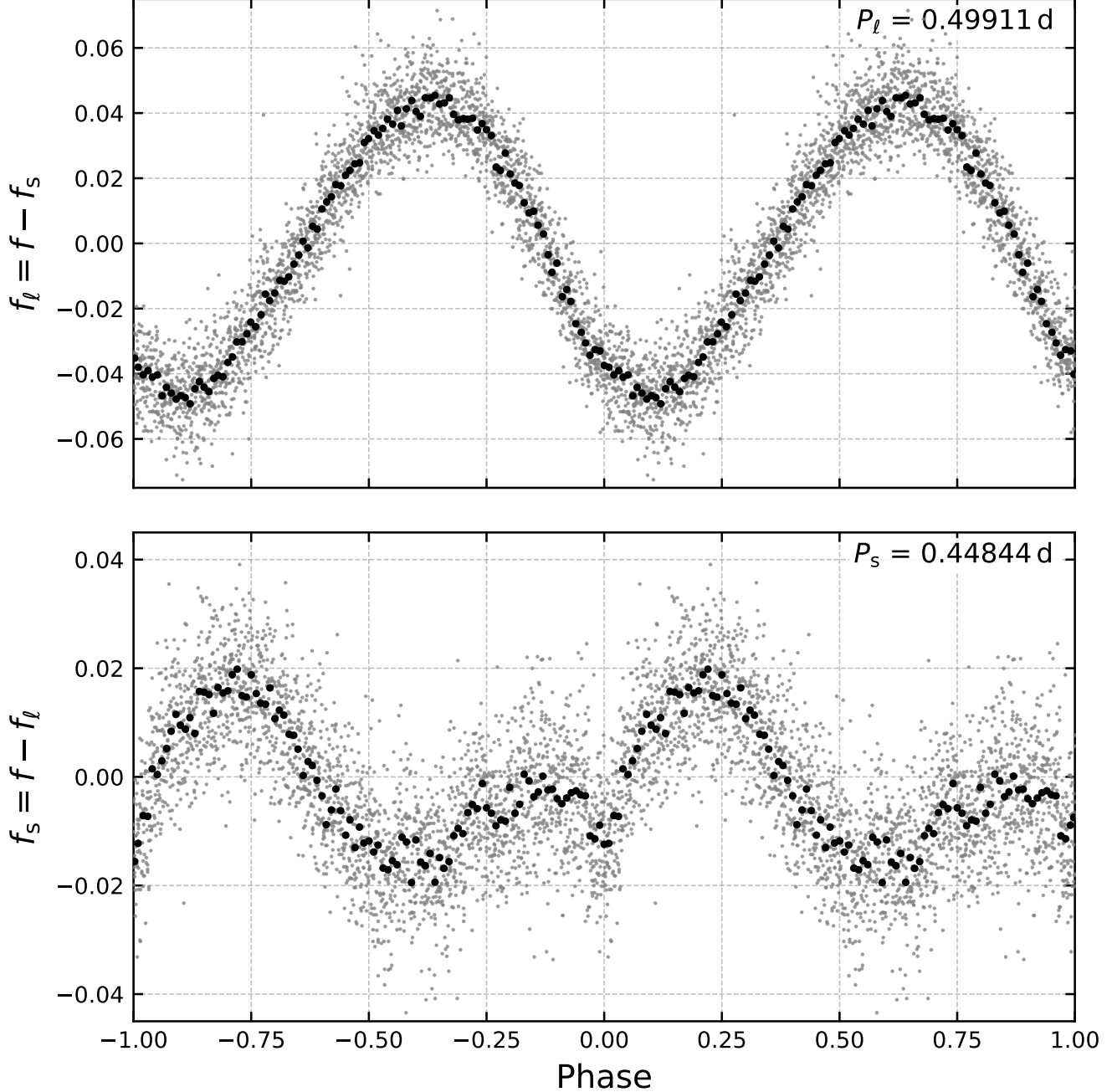
Figure 3. Phase-folded long and short-period signals. *Top*: Long-period signal, as in Figure 1. *Bottom*: Short-period signal. The reference phase is set to the "planetary" dip. Gray points are the 10 minute cadence `PDCSAP` flux. Black points are binned to 100 points per period.

itself and its phase. For this case, we therefore fitted 14 free parameters.

We implemented and fitted the models using `PyMC3`, which is built on `theano` (Salvatier et al. 2016; Theano Development Team 2016). For the Fourier terms, we used the default math operators. For the exoplanet transit, we used the model and derivatives implemented in `exoplanet` (Foreman-Mackey et al. 2020). Our priors are listed in Table 2. To speed up the fitting, we re-sampled the cleaned 2 minute lightcurves to 10 minute binning. We correspond-

ingly scaled the uncertainties in the flux measurements by a factor of $\sqrt{5}$. Before sampling, we initialized each model to the maximum a posteriori (MAP) solution. We then sampled using `PyMC3`'s gradient-based No-U-Turn Sampler (Hoffman & Gelman 2014), and used $\hat{R}$ as our convergence diagnostic (Gelman & Rubin 1992). We tested our ability to successfully recover injected parameters using synthetic data, before fitting the PTFO 8-8695 lightcurves.

3.3. Fitting Results

We considered nine models, with the number of harmonics per frequency N and M ranging from one to three. To select our preferred model, we used the Bayesian information criterion (Table 1). The model with the lowest BIC had two harmonics at the short 10.74 hr period, and two harmonics at the long 11.96 hr period. The next-best model had an additional harmonic at the longer period ($M = 3$), but was otherwise identical. All nine models have reduced χ^2 ranging between 1.37 and 1.51, which suggests a plausible though imperfect agreement between the data and fitting results. The best-fit parameters for the lowest BIC model are given in Table 2.

To explore where each model succeeded and failed, we split the raw signal into its respective components (Figures 1 and 2). We also examined the phase-folded signals (Figure 3).

In every model, the 11.96 hr variability is a simple sinusoid with peak-to-peak amplitude $\approx$10%. The 10.74 hr variability is always more complex. A dip of depth $\approx$1.2%, fit in our model as a transit, lasts $\approx$0.75 hours. Superposed on the dip is a slightly asymmetric sinusoid with peak-to-peak amplitude of about 4%. The asymmetric sinusoid peaks near phase 0.25, and reaches minimum brightness between phases -0.5 and -0.25. The flux at phase ≈ -0.33 shows what could be a discontinuous jump, shortly after reaching minimum (Figure 3). This jump was visible in each of the nine models we considered.

The periodogram of the final residual (Figure 1 bottom row) shows a weakly significant, poorly resolved peak at $\approx$8 days, consistent with the visual impression in the time domain that there could be a weak long-period signal present.

4. BINARITY ANALYSIS

4.1. *Visual Binarity*

The TESS pixels are $\approx$ 21" per side. Before making any interpretations, we needed to consider whether light from known neighboring stars could have affected the photometry. The scene is shown in Figure 4. In the upper panels, the pixels used to measure the background level in the SPOC lightcurve are indicated with an 'X' hatch, and the pixels used in the final lightcurve aperture are shown with the '/' hatch.

The target star, PTFO 8-8695 (TIC 264461976), has a T-band magnitude of 14.0, and its position is shown with a star. The other (unlabeled) star inside the target aperture, TIC 264461979, has $T = 16.8$ and so cannot contribute a signal with relative amplitude 10%. The only neighbor that is sufficiently close and bright that its light might contaminate the target star is TIC 264461980, with $T = 14.8$, which we dub "Star A". Star A is 23.6" NW of our target, and based on the magnitude difference could contribute up to 48% the flux of our target star, PTFO 8-8695.

Because PTFO 8-8695 was previously identified to have periodicity consistent with our measurement of P_s, our main concern regarding blending was the degree to which we could be certain that the long-period signal at P_ℓ also originated from PTFO 8-8695. We took two approaches to verifying the source of the long-period signal.
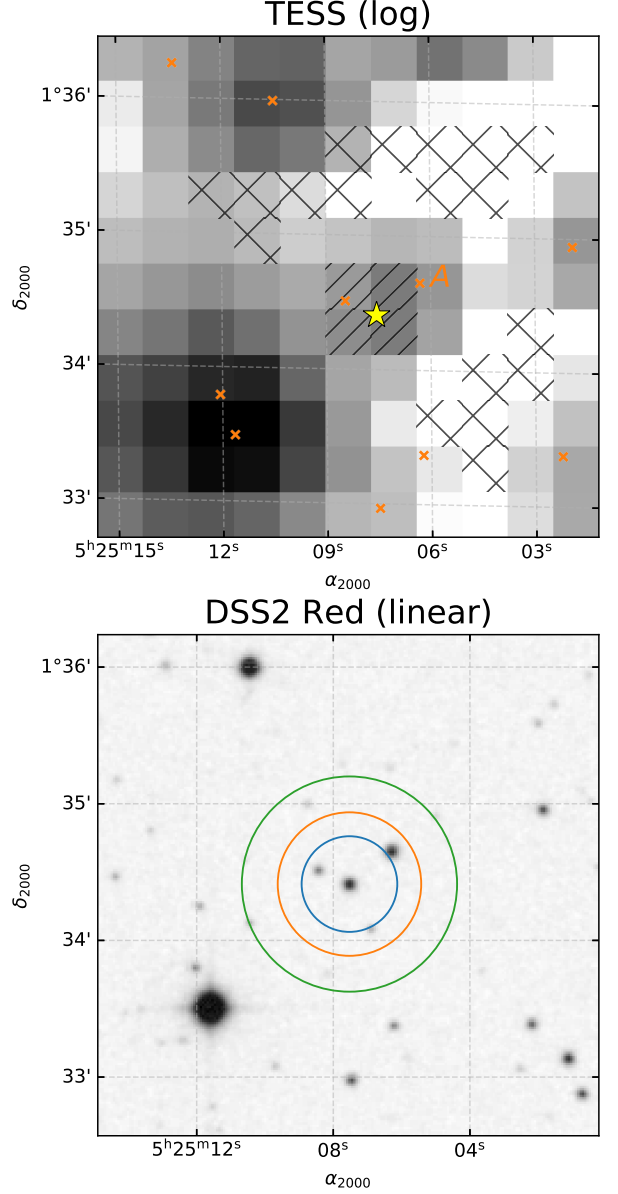
Figure 4. Scene used for blend analysis. *Top:* Mean TESS image of PTFO 8-8695 over Sector 6, with a log-stretch. The position of PTFO 8-8695 is shown with a yellow star. Neighbors with $T < 17$ are shown with orange crosses. The apertures used to measure the background and target star flux are shown with X and / hatches, respectively. *Bottom:* Digitized Sky Survey R-band image of the same field, with a linear stretch. The circles show apertures of radii 1, 1.5, and 2.25 pixels used in part of our blend analysis. The pixel level TESS data show that "Star A" does not contribute variability at either of the two observed periods (see Section 4.1).

First, we examined the CDIPS FFI lightcurves of the target, which were available on MAST (Bouma et al. 2019). The maximal peak-to-peak beat amplitude was constant across apertures of radii 1, 1.5, and 2.25 pixels to visual precision ($\lesssim$ 1%). If Star A were the source of the long-period variability, we would expect the peak variability amplitude to

be smallest in the 1 pixel aperture, based on the separation of the sources (Figure 4, bottom). From this test alone, it seems unlikely that Star A is the source of the long-period signal.

Second, we examined the 2-minute lightcurve of each pixel in the scene individually. We opted to use the interactive tools implemented in `lightkurve` (Lightkurve Collaboration et al. 2018). If Star A were the source of the long-period variability, we would expect the pixels nearest to Star A to show a sinusoidal signal with amplitude exceeding 10%. The data do not support this possibility. The pixel directly below Star A does not clearly show the sinusoidal variability, and the peak-to-peak variability in that pixel is $\lesssim 8\%$. In contrast, the south-easternmost pixel within PTFO 8-8695's aperture (the pixel furthest from Star A that was used in the optimal aperture) shows the P_ℓ sinusoidal variability signal at $\approx 14\%$ amplitude. We conclude that within the resolution of the Gaia DR2 source catalog, the P_s and P_ℓ signals originate from PTFO 8-8695. From Ziegler et al. (2018), we can surmise that stellar companions wider than ≈ 1" (349 AU) and within $\Delta G \approx 3$ magnitudes of PTFO 8-8695 would have likely been detected through this approach.

van Eyken et al. (2012) obtained stronger constraints on possible stellar companions using the NIRC2 camera on Keck II. They reported 3σ H-band magnitude difference limits of 4.3, 6.4, and 8.9 at angular separations of 0.25, 0.5, and 1.0 arcseconds (87, 175, and 349 AU). They also detected a point-source, not present in Gaia DR2, 7.0 magnitudes fainter than the target, and 1.8″ north-east. Due to the brightness difference, this coincident star[2] cannot be the source of our signals.

While long-baseline radial velocity measurements could provide complimentary lower limits on companion masses and separations, the RV data for PTFO 8-8695 are rather poor owing to the stellar faintness. The longest single-instrument baseline in the literature appears to be 5 Keck/HIRES measurements acquired over 10 days in April 2011 by van Eyken et al. (2012). The RV RMS over that 10 day span was $1.6\,\mathrm{km\,s^{-1}}$, consistent with the measurement precision. Though Yu et al. (2015) acquired 22 further Keck/HIRES observations over one night in December 2013, these points seem to not have been reduced to velocities. Further Keck/HIRES measurements of this target could confirm or refute the existence of possible binary companions.

4.2. *Photometric Binarity*

Aside from visual binarity, we can also check the Gaia data for photometric binarity. To assemble a set of stars coeval with PTFO 8-8695, we used the 25 Ori-1 members identified by Kounkel et al. (2018), and discussed in Section 2.2.2.

To define a set of non-member stars that nonetheless had comparable selection functions, we defined a reference "neighborhood" as the group of at most 10^4 randomly se-

lected non-member stars within 5 standard deviations of the mean 25 Ori-1 right ascension, declination, and parallax. We queried Gaia DR2 for these stars using `astroquery` (Ginsburg et al. 2018). This yielded 1,819 neighbors. While some of these stars may indeed be members of the Orion complex, or even of 25 Ori-1, enforcing this cut on positions and parallaxes ensures that we are querying stars with comparable amounts of interstellar reddening.

We examined the resulting five-dimensional right ascension, declination, proper motions, and parallaxes. The first point we noted was that 25 Ori-1 was a clearly defined overdensity in each dimension—the cluster exists, and is distinct from the neighborhood. PTFO 8-8695 was also within the cluster in each of these projected dimensions.

Given our detection of two separate signals, whether PTFO 8-8695 could be a photometric binary was of great interest. Figure 5 shows the HR diagram we constructed to assess this issue. The diagram shows that PTFO 8-8695 is ≈ 0.75 magnitudes brighter than the average 25 Ori-1 star of the same color. In other words, it is about twice as bright. It also seems to be coincident with the photometric binary track of the cluster, which has a few other stars.

The implication is that either *(i)* PTFO 8-8695 is notably younger than the kinematically identical 25 Ori-1 members, or *(ii)* PTFO 8-8695 is a photometric binary. Since there is no a priori reason to suspect an age difference, but we have resolved two separate photometric signals, we favor the binary interpretation.

4.3. *Astrometric Binarity*

A separate possible line of evidence for binarity is the Gaia DR2 astrometry. As noted in Section 2, the Gaia DR2 solution for PTFO 8-8695 shows a 10.3σ astrometric excess. This astrometric excess indicates the degree to which a single-source model fails to explain the observed astrometric measurements. Specifically, the single-source astrometric model yielded $\chi^2 = 325.2$. There are 121 astrometric measurements, and 5 free parameters, and therefore 116 degrees of freedom. The reduced χ^2 is 2.80. The majority of stars with comparable brightness in Gaia do not show such poor goodness-of-fit (Lindegren et al. 2018, Appendix A).

Potential explanations for the poor astrometric fit include photometric variability and unresolved stellar binarity (*e.g.*, Rizzuto et al. 2018; Belokurov et al. 2020). If photometric variability were the cause, we would expect comparably faint stars in the same kinematic group of Orion to show similar astrometric excesses, as the majority of young stars are highly variable.

Using the same 149 members in the 25 Ori-1 subgroup from Kounkel et al. (2018), we calculated the reduced χ^2 for each member. The lower panel of Figure 5 shows the resulting values, as a function of stellar brightness. PTFO 8-8695 is in the upper 90th percentile of stars showing astrometric excesses within the 25 Ori-1 group. Relative to other M-dwarf group members with comparable brightnesses and variability characteristics, PTFO 8-8695 still stands out as behaving astrometrically poorly. Ultimately, we will have to wait for

---

[2] This companion was claimed to be a potential planetary-mass object (Schmidt et al. 2016). Subsequent analysis of its colors showed that it is a background star (Lee & Chiang 2018).
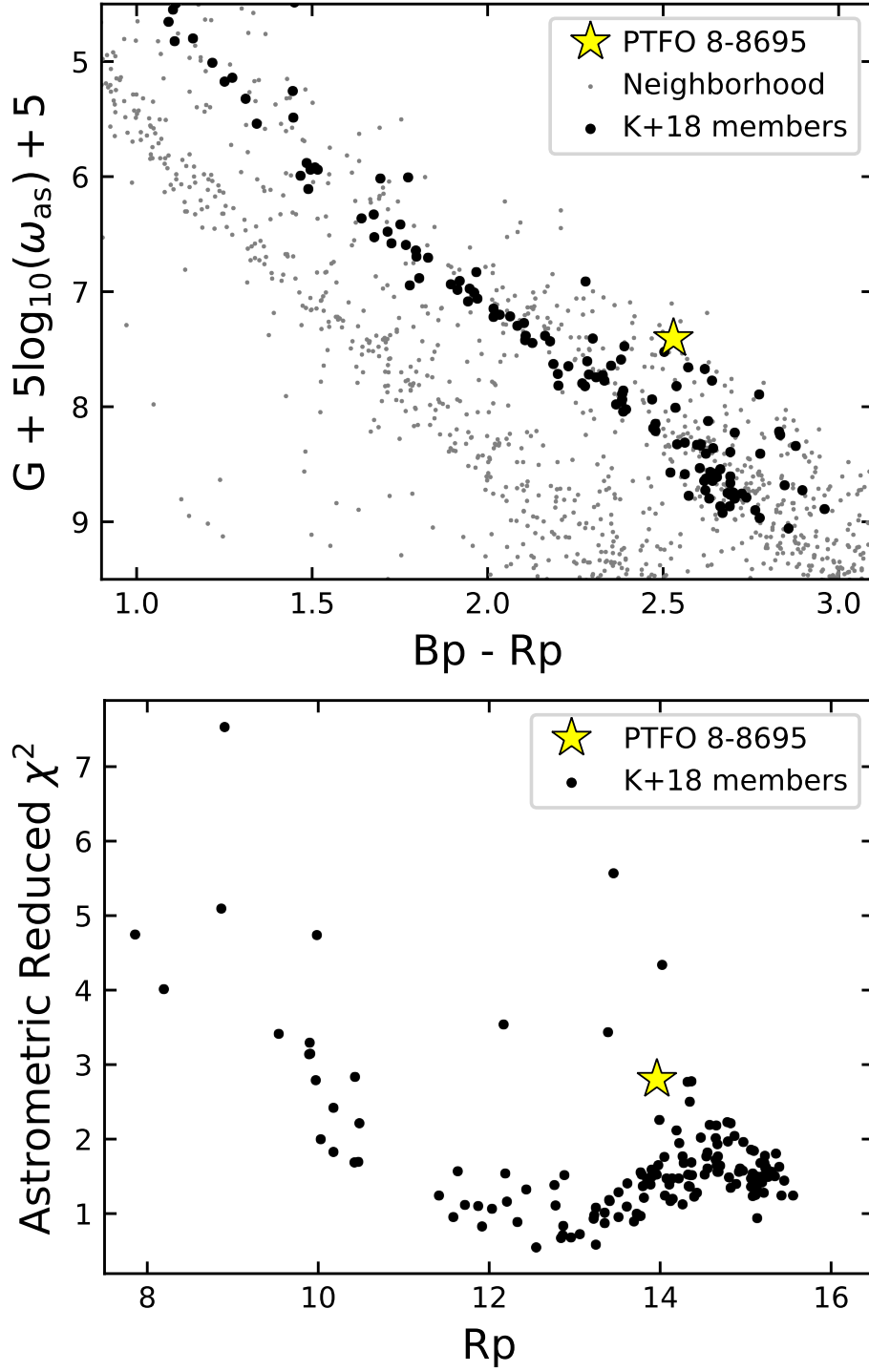
Figure 5. Evidence for binarity in PTFO 8-8695. *Top: Hertzsprung-Russell diagram of PTFO 8-8695 and late-type members of 25 Ori-1.* Members of the 25 Ori-1 group (black circles) were identified by Kounkel et al. (2018) through clustering on six-dimensional Gaia DR2 and APOGEE-2 data. The "neighborhood" (gray circles) is non-member stars within 5 standard deviations of the mean 25 Ori-1 right ascension, declination, and parallax. It contains members of the Orion complex with its full spread of ages, in addition to field interlopers. *G* denotes Gaia broadband magnitudes, *Bp* Gaia blue, *Rp* Gaia red, and ω_{as} the parallax in arcseconds. The *x*-axis limits have been set to show only K and M dwarf members, to accentuate PTFO 8-8695's separation from the single-star sequence. *Bottom: Astrometric goodness-of-fit versus Rp magnitude for 25 Ori-1 members.* The single-source astrometric model provides a poor fit, which could be due to stellar variability or binarity.

the full release of the nominal Gaia mission to definitively determine whether the astrometric excess is caused by stellar binarity or photometric variability. Nonetheless this result suggests that stellar binarity is indeed the root cause, because other member stars have identical variability characteristics but do not show such a large astrometric excess.

5. DISCUSSION

5.1. *Long period sinusoid*

The standard interpretation for 11.96 hour sinusoidal modulations of a pre-main-sequence M dwarf is stellar rotation. This is the dominant signal in the system with 10% amplitude, and there is no evidence to suggest that this signal has any other origin.

The discovery study by van Eyken et al. (2012) saw an alias of the same signal (*e.g.*, their Figure 7), and identified it as a periodogram peak at 0.9985 ± 0.0061 days. They ascribed it to their observing cadence, because of its close correspondence to the sidereal day. While the TESS data can show significant reflected light from the Earth (*e.g.*, Luger et al. 2019), our pixel-level analysis showed that the signal is specific to only pixels near PTFO 8-8695, and no other pixels. We therefore conclude that the signal is not a systematic.

We are not the first to reach the conclusion that the long period sinusoidal modulation is astrophysical. A study by Koen (2015) identified the same modes and aliases as van Eyken et al. (2012), but argued that the signal was astrophysical (however they were still unsure of the exact period). Using photometry from the YETI global telescope network, Raetz et al. (2016) eventually came to the conclusion that the 0.50 d signal was indeed from stellar rotation. The TESS data strongly support this conclusion.
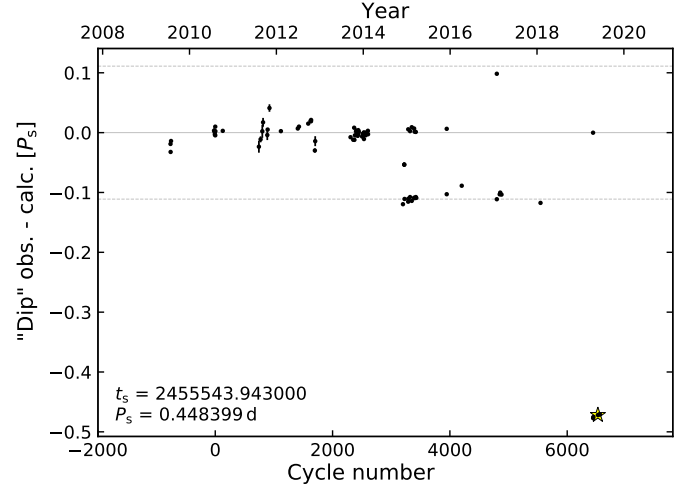
5.2. *Short period dip*

The TESS lightcurve shows a dip that lasts about 45 minutes, and seems to re-occur every 10.74 hours (Figures 1, 2, 3). The dip duration is roughly the same as that observed by previous investigators (van Eyken et al. 2012; Yu et al. 2015). The 1.2% depth is similar to what has been observed in the near-infrared (Onitsuka et al. 2017). However the dip depth seems likely to have evolved over time between being not present at all, to a maximum of ≈5% (Koen 2015; Yu et al. 2015; Tanimoto et al. 2020, *e.g.*,).

One particularly interesting feature of the dip is its epoch. Over the past decade, many investigators have observed PTFO 8-8695. Its dips do not always occur on a perfectly linear ephemeris (Yu et al. 2015). In fact, Tanimoto et al. (2020) recently provided stark evidence for different behavior altogether: over a time-span of years, the dip "splits" into distinct groups at particular repeating phases. See for instance their Figures 2 through 4. Fitting a decade of observations, they provided the following linear ephemeris.

$$t_0 \; \mathrm{BJD_{TDB}} = 2455543.943 \pm 0.002 \qquad (4)$$

$$P = 0.4483993 \pm 0.0000006 d. \qquad (5)$$

In Figure 6, we show the phase of the dip we detect in the TESS data, relative to their ephemeris. It agrees with

Figure 6. Timing residuals for PTFO 8-8695b from a decade of monitoring. Black points are times of dips, minus the indicated linear ephemeris. The *y*-axis is given in units of phase for the short-period signal. The star shows the binned TESS ephemeris. Dips have been observed by van Eyken et al. (2012), Ciardi et al. (2015), Yu et al. (2015), Raetz et al. (2016), Onitsuka et al. (2017), and Tanimoto et al. (2020). Certain dips (*e.g.*, the one at phase 0 in mid-2019) are consistent with noise, and were likely reported because something was *expected*, rather than convincingly *observed*. Horizontal dashed lines are drawn at $\pm (P_\ell - P_s)/P_s$, highlighting either a numerical coincidence or an observational bias. The orbital phase observed by TESS is consistent with that of Tanimoto et al. (2020), and quite different from the original phase.

the independent December 2018 measurements by Tanimoto et al. (2020): the dip has drastically shifted phase over the past decade.

Figure 6 shows two additional strange features: *(i)* multiple dips per cycle, and *(ii)* a set of dips numerically coincident with phase $(P_\ell - P_s)/P_s$. The observation of multiple dips per cycle in 2015 seems to have been detected by both Yu et al. (2015) and Tanimoto et al. (2020). It therefore seems credible. Inspecting the Tanimoto et al. (2020) lightcurves, the claim of multiple dips per cycle in December 2018 at phase 0 and -0.47 seems much less plausible—the phase -0.47 dips are strongly detected, while the suggested phase 0 dip is not clearly present.

We are not sure what to make of the numerical coincidence. The ratio of long to short periods is roughly 10:9, which does produce a beat. However it is not clear that this would obviously translate into an observational bias unless by some fluke three season's worth of observations managed to only observe every ninth dip. This is of course not the case, and we therefore leave this curiosity as observation *sans* interpretation.

5.3. *Short period out-of-dip modulation*

If there were a giant planet transiting PTFO 8-8695, it would tidally distort the host star, and cause ellipsoidal photometric modulations. The amplitude of the ellipsoidal dis-

tortion for a $1 M_{\rm Jup}$ companion would be about 1400 ppm (Shporer 2017). This is significantly larger than the typical ellipsoidal modulation induced by close-in giant planets because the host star is puffy, and still on the pre-main-sequence. For our estimate, we assumed $R_\star = 1.39 R_\odot$, and $M_\star = 0.39 M_\odot$ (van Eyken et al. 2012).

Our preferred model does detect a significant ellipsoidal signal, parametrized as the "B_1" component. The amplitude of the signal is $0.53 \pm 0.06\%$ (see Table 2). Interpreted as being caused by a planet, it would imply a minimum planet mass $M_{\rm p} \sin i$ of $3.8 M_{\rm Jup}$.

6. PHYSICAL INTERPRETATION

Given the evidence, we believe that PTFO 8-8695 is a binary M dwarf in which one star shows the "long" rotation signal, and the other is showing "transient dipping" that has also been observed in other young M dwarfs.

Many other young M-dwarf photometric binaries have been observed in *e.g.,* Upper Sco and the Pleiades to show multiple periods (Rebull et al. 2018; Stauffer et al. 2018). Typically, the periods are both rotational modulation.

However, occasionally one or both periods can be "scallop-shell" variability, *e.g.*, EPIC 203956650 in ρ Oph (Rebull et al. 2018).

There are

The gas in the disks is gone (CITE). The upper limits on the SED from Yu et al. (2015) imply X, Y, Z. The stars are therefore presumably no longer "magnetically locked" to their disks. This is consistent with the $\approx$half-day periodicities of both signals. In the broader context of rapidly rotating young M-dwarfs, "magnetic locking" causes classical disked T-Tauri stars tend to rotate more *slowly*, and almost none have periods less than two days (*e.g.*, Rebull et al. 2020).

The main physical question is what is causing the "transient dipping". This is an unsolved problem not only for PTFO 8-8695 but also for an entire class of young rapidly rotating M-dwarfs

The roughly half-day periods of both signals imply that

7. CONCLUSIONS

PTFO 8-8695 was previously thought to potentially host a hot Jupiter. The TESS lightcurve of PTFO 8-8695 showed a number of new features, many of which seem to disfavor the hot Jupiter interpretatation. The TESS data showed two key pieces of evidence.

1. *Two periodic signals.* The "long" signal is a 10% peak-to-peak sinusoidal modulation repeating every 11.96 hours. The "short" signal is a 4% peak-to-peak complex modulation repeating every 10.74 hours. It is composed of a dip, plus at least two harmonics. The signals beat, and therefore cannot be an artifact linked to data processing.

2. *A dip at the wrong orbital phase.* The clearest dip in the "short" signal was consistent with recent observa-

tions by Tanimoto et al. (2020), and differed from the discovery epoch by 5.14 hours.

The physical mechanism responsible for all these features remains a matter of speculation. With that said, the TESS data support new arguments against the planetary interpretation of PTFO 8-8695. First, if the long signal is caused by starspot modulation, and the short signal by a transiting planet, what causes the additional complex modulations seen at the short, "orbital", period?

Similarly, if the planet truly orbits every 10.74 hours, while the star's equator spins every 11.96 hours, the situation is clearly Darwin unstable.

Given the available evidence, PTFO 8-8695 seems consistent with the "transient dipping" phenomenology observed in many young M dwarfs. It seems rather unlikely to be a planet.

Software: `astrobase` (Bhatti et al. 2018), `astropy` (Astropy Collaboration et al. 2018), `astroquery` (Ginsburg et al. 2018), `corner` (Foreman-Mackey 2016), `exoplanet` (Agol et al. 2019) `exoplanet` (Foreman-Mackey et al. 2020), and its dependencies (Agol et al. 2019; Kipping 2013; Luger et al. 2019; Theano Development Team 2016). `IPython` (Pérez & Granger 2007), `lightkurve` (Lightkurve Collaboration et al. 2018), `matplotlib` (Hunter 2007), `MESA` (Paxton et al. 2011, 2013, 2015) `numpy` (Walt et al. 2011), `pandas` (McKinney 2010), `PyMC3` (Salvatier et al. 2016), `radvel` (Fulton et al. 2018), `scipy` (Jones et al. 2001).
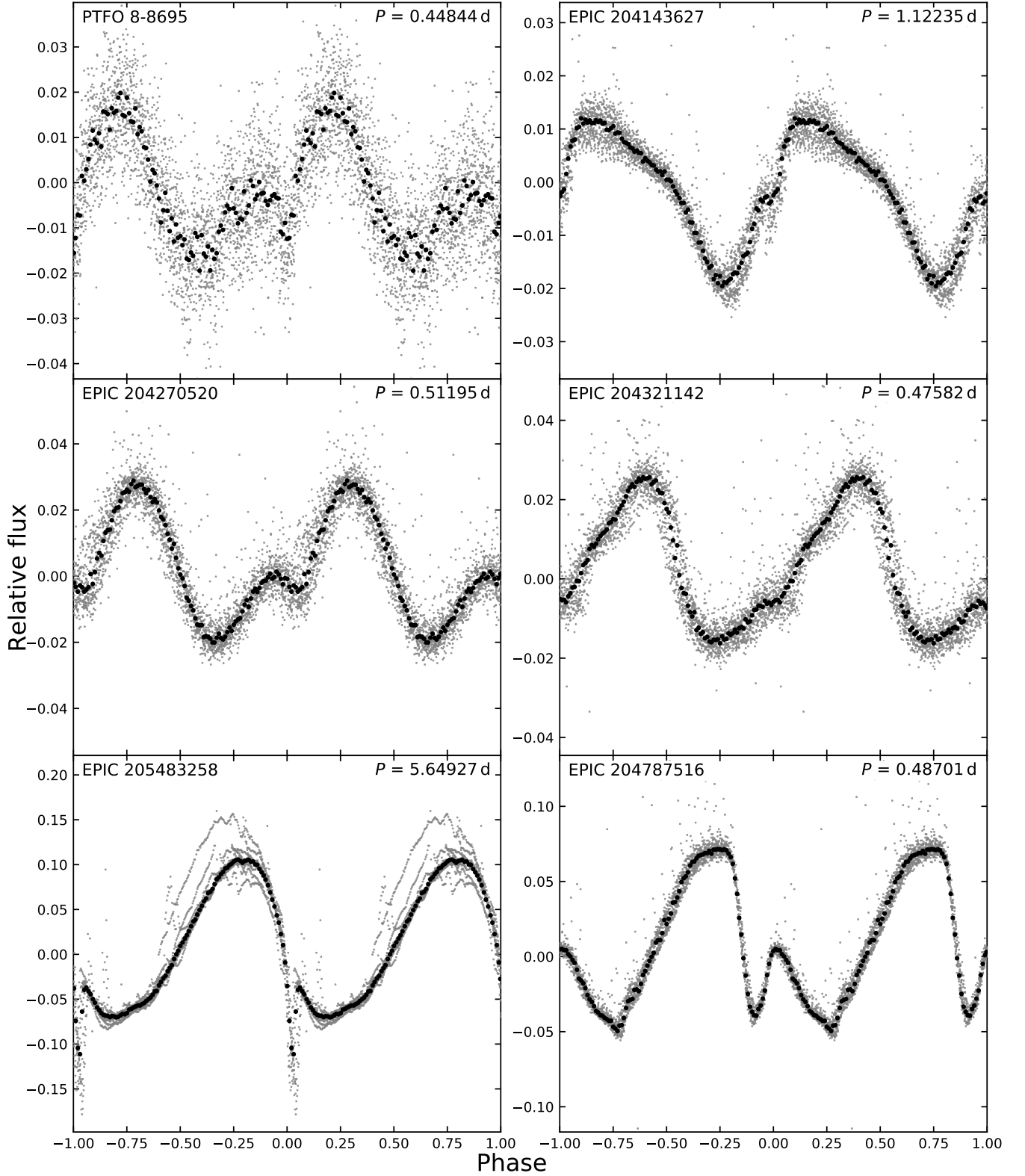
Figure 7. PTFO 8-8695 and its brethren. Five transient and persistent flux dip stars, selected based on their visual similarity to the short-period signal in PTFO 8-8695, are as follows. EPIC 204143627, 1.1250d, dips change depth too EPIC 204321142 Usco flux dip, 0.476d EPIC 204270520 USco flux dip, 0.512d RIK-210 = EPIC 205483258 EPIC 204787516 USco flux dip or possible? EB, 0.487d We found these objects through studies by Stauffer et al. (2017), David et al. (2017), and Rebull et al. (2018).

Table 1. Model Comparison.

Description	N	M	N_{data}	N_{param}	χ^2	χ^2_{red}	BIC	ΔBIC
Favored	2	2	2585	17	3523.6	1.372	3657.2	0.0
Somewhat favored	2	3	2585	19	3512.7	1.369	3662.0	4.8
Disfavored	3	2	2585	19	3543.1	1.381	3692.4	35.2
—	3	3	2585	21	3536.8	1.379	3701.9	44.6
—	1	2	2585	15	3680.0	1.432	3797.9	140.7
—	1	3	2585	17	3670.2	1.429	3803.8	146.6
—	2	1	2585	15	3700.9	1.440	3818.8	161.6
—	3	1	2585	17	3710.2	1.445	3843.7	186.5
—	1	1	2585	13	3872.7	1.506	3974.8	317.6

NOTE— N and M are the number of harmonics at the short and long periods, respectively. N_{data} is the number of fitted flux measurements. N_{param} is the number of free parameters in the model. The Bayesian information criterion (BIC) and the difference from the maximum ΔBIC are also listed.

Table 2. Best-fit model priors and posteriors.

Param.	Prior	Mean	Std. Dev.	3%	97%
P_{s}	$\mathcal{N}(0.4485; 0.0010)$	0.4484732	0.0000857	0.4483170	0.4486367
$t_{\text{s}}^{(1)}$	$\mathcal{N}(0.438096; 0.0020)$	0.4384733	0.0017440	0.4349337	0.4415021
$R_{\text{p}}/R_{\star}$	$\mathcal{N}(0.1100; 0.0033)$	0.11	0.00308	0.10452	0.11599
b	$\mathcal{U}(0; 1+R_{\text{p}}/R_{\star})$	0.7736	0.0756	0.6346	0.8993
u_1	(2)	0.683	0.477	0.001	1.546
u_2	(2)	0.004	0.417	-0.793	0.727
Mean	$\mathcal{U}(-0.01; 0.01)$	-0.000885	0.000440	-0.001745	-0.000088
ω_{s}	$2\pi/P_{\text{s}}$	14.01017	0.00268	14.00506	14.01505
$A_{\text{s},0}$	$\mathcal{U}(-0.02; 0.02)$	0.008903	0.000705	0.007569	0.010277
$B_{\text{s},0}$	$\mathcal{U}(-0.02; 0.02)$	0.009985	0.000751	0.008504	0.011289
$A_{\text{s},1}$	$\mathcal{U}(-0.02; 0.02)$	0.001649	0.000696	0.000331	0.002884
$B_{\text{s},1}$	$\mathcal{U}(-0.02; 0.02)$	-0.005267	0.000606	-0.006491	-0.004203
ϕ_{ℓ}	$\mathcal{U}(1.3721; 2.1575)$	1.74324	0.22254	1.38274	2.08874
ω_{ℓ}	$\mathcal{N}(12.6054; 0.1261)$	12.588581	0.002040	12.584940	12.592450
$A_{\ell,0}$	$\mathcal{U}(-0.06; 0.06)$	0.037785	0.005150	0.028728	0.045214
$B_{\ell,0}$	$\mathcal{U}(-0.06; 0.06)$	0.022288	0.008592	0.008066	0.0359
$A_{\ell,1}$	$\mathcal{U}(-0.02; 0.02)$	0.002326	0.000756	0.000857	0.003658
$B_{\ell,1}$	$\mathcal{U}(-0.02; 0.02)$	-0.002197	0.000744	-0.003512	-0.000743

(1) To convert mean TESS mid-transit time to BJD$_{\text{TDB}}$, add 2458468.2. (2) Quadratic limb-darkening prior from Kipping (2013), implemented by Foreman-Mackey et al. (2020).

REFERENCES

Agol, E., Luger, R., & Foreman-Mackey, D. 2019, arXiv e-prints, 1908.03222

Astropy Collaboration, Price-Whelan, A. M., Sipőcz, B. M., et al. 2018, AJ, 156, 123

Barnes, J. W., van Eyken, J. C., Jackson, B. K., Ciardi, D. R., & Fortney, J. J. 2013, The Astrophysical Journal, 774, 53

Belokurov, V., Penoyre, Z., Oh, S., et al. 2020, arXiv:2003.05467 [astro-ph], arXiv: 2003.05467

Bhatti, W., Bouma, L. G., & Wallace, J. 2018, astrobase, https://doi.org/10.5281/zenodo.1469822

Blanton, M. R., Bershady, M. A., Abolfathi, B., et al. 2017, The Astronomical Journal, 154, 28

Bouma, L. G., Hartman, J. D., Bhatti, W., Winn, J. N., & Bakos, G. Á. 2019, ApJS, 245, 13

Briceño, C., Calvet, N., Hernández, J., et al. 2005, The Astronomical Journal, 129, 907

Briceño, C., Hartmann, L., Hernández, J., et al. 2007a, The Astrophysical Journal, 661, 1119

Briceño, C., Preibisch, T., Sherry, W. H., et al. 2007b, Protostars and Planets V, 345

Briceño, C., Calvet, N., Hernández, J., et al. 2019, The Astronomical Journal, 157, 85

Ciardi, D. R., Eyken, J. C. v., Barnes, J. W., et al. 2015, The Astrophysical Journal, 809, 42, publisher: IOP Publishing

Cottle, J., Covey, K. R., Suárez, G., et al. 2018, The Astrophysical Journal Supplement Series, 236, 27

Cropper, M., Katz, D., Sartoretti, P., et al. 2018, Astronomy and Astrophysics, 616, A5

David, T. J., Petigura, E. A., Hillenbrand, L. A., et al. 2017, The Astrophysical Journal, 835, 168

Evans, D. W., Riello, M., De Angeli, F., et al. 2018, Astronomy and Astrophysics, 616, A4

Foreman-Mackey, D. 2016, The Journal of Open Source Software, 24

Foreman-Mackey, D., Czekala, I., Luger, R., et al. 2020, exoplanet-dev/exoplanet v0.2.6

Fulton, B. J., Petigura, E. A., Blunt, S., & Sinukoff, E. 2018, PASP, 130, 044504

Gaia Collaboration, Prusti, T., de Bruijne, J. H. J., et al. 2016, A&A, 595, A1

Gaia Collaboration, Brown, A. G. A., Vallenari, A., et al. 2018, A&A, 616, A1

Gelman, A., & Rubin, D. B. 1992, Statistical Science, 7, 457, publisher: Institute of Mathematical Statistics

Ginsburg, A., Sipocz, B., Madhura Parikh, et al. 2018, Astropy/Astroquery: V0.3.7 Release

Gunn, J. E., Siegmund, W. A., Mannery, E. J., et al. 2006, The Astronomical Journal, 131, 2332

Hernández, J., Calvet, N., Briceño, C., et al. 2007, The Astrophysical Journal, 671, 1784

Hoffman, M. D., & Gelman, A. 2014, Journal of Machine Learning Research, 15, 1593

Howarth, I. D. 2016, Monthly Notices of the Royal Astronomical Society, 457, 3769

Hunter, J. D. 2007, Computing in Science & Engineering, 9, 90

Jeffries, R. D., Maxted, P. F. L., Oliveira, J. M., & Naylor, T. 2006, Monthly Notices of the Royal Astronomical Society, 371, L6

Jenkins, J. M., Twicken, J. D., McCauliff, S., et al. 2016, Software and Cyberinfrastructure for Astronomy IV, 9913, 99133E

Johns-Krull, C. M., Prato, L., McLane, J. N., et al. 2016, The Astrophysical Journal, 830, 15

Jones, E., Oliphant, T., Peterson, P., et al. 2001, Open source scientific tools for Python

Kamiaka, S., Masuda, K., Xue, Y., et al. 2015, Publications of the Astronomical Society of Japan, 67, 94

Kipping, D. M. 2013, mnras, 435, 2152

Koen, C. 2015, Monthly Notices of the Royal Astronomical Society, 450, 3991

Kounkel, M., Covey, K., Suárez, G., et al. 2018, The Astronomical Journal, 156, 84

Lee, C.-H., & Chiang, P.-S. 2018, The Astrophysical Journal Letters, 852, L24

Lightkurve Collaboration, Cardoso, J. V. d. M., Hedges, C., et al. 2018, Lightkurve: Kepler and TESS time series analysis in Python, Astrophysics Source Code Library, ascl:1812.013

Lindegren, L., Hernández, J., Bombrun, A., et al. 2018, Astronomy & Astrophysics, 616, A2

Lomb, N. R. 1976, Astrophysics and Space Science, 39, 447

Luger, R., Agol, E., Foreman-Mackey, D., et al. 2019, aj, 157, 64

Luger, R., Bedell, M., Vanderspek, R., & Burke, C. J. 2019, arXiv:1903.12182 [astro-ph], arXiv: 1903.12182

Majewski, S. R., Schiavon, R. P., Frinchaboy, P. M., et al. 2017, The Astronomical Journal, 154, 94

McKinney, W. 2010, in Proceedings of the 9th Python in Science Conference, ed. S. van der Walt & J. Millman, 51

Onitsuka, M., Fukui, A., Narita, N., et al. 2017, Publications of the Astronomical Society of Japan, 69

Paxton, B., Bildsten, L., Dotter, A., et al. 2011, ApJS, 192, 3

Paxton, B., Cantiello, M., Arras, P., et al. 2013, ApJS, 208, 4

Paxton, B., Marchant, P., Schwab, J., et al. 2015, ApJS, 220, 15

Pérez, F., & Granger, B. E. 2007, Computing in Science and Engineering, 9, 21

Raetz, S., Schmidt, T. O. B., Czesla, S., et al. 2016, Monthly Notices of the Royal Astronomical Society, 460, 2834

Rebull, L. M., Stauffer, J. R., Cody, A. M., et al. 2020

—. 2018, The Astronomical Journal, 155, 196

Ricker, G. R., Winn, J. N., Vanderspek, R., et al. 2015, Journal of Astronomical Telescopes, Instruments, and Systems, 1, 014003

Rizzuto, A. C., Vanderburg, A., Mann, A. W., et al. 2018, arXiv:1808.07068 [astro-ph], arXiv: 1808.07068

Salvatier, J., Wieckiâ, T. V., & Fonnesbeck, C. 2016, PyMC3: Python probabilistic programming framework

Scargle, J. D. 1982, The Astrophysical Journal, 263, 835

Schmidt, T. O. B., Neuhäuser, R., Briceño, C., et al. 2016, Astronomy and Astrophysics, 593, A75

Shporer, A. 2017, PASP, 129, 072001

Smith, J. C., Morris, R. L., Jenkins, J. M., et al. 2017a, Kepler Science Document, 7

Smith, J. C., Stumpe, M. C., Jenkins, J. M., et al. 2017b, Kepler Science Document, 8

Stassun, K. G., Oelkers, R. J., Pepper, J., et al. 2018, AJ, 156, 102

Stassun, K. G., Oelkers, R. J., Paegert, M., et al. 2019, arXiv:1905.10694 [astro-ph], arXiv: 1905.10694

Stauffer, J., Rebull, L. M., Cody, A. M., et al. 2018, The Astronomical Journal, 156, 275, publisher: American Astronomical Society

Stauffer, J., Cameron, A. C., Jardine, M., et al. 2017, The Astronomical Journal, 153, 152

Tanimoto, Y., Yamashita, T., Ui, T., et al. 2020, PASJ, arXiv:2001.00148 [astro-ph.EP]

Tenenbaum, P., & Jenkins, J. 2018, TESS Science Data Products Description Document, EXP-TESS-ARC-ICD-0014 Rev D, https://archive.stsci.edu/missions/tess/doc/EXP-TESS-ARC-ICD-TM-0014.pdf

Theano Development Team. 2016, arXiv e-prints, abs/1605.02688

van Eyken, J. C., Ciardi, D. R., von Braun, K., et al. 2012, The Astrophysical Journal, 755, 42

VanderPlas, J. T., & Ivezić, Z. 2015, The Astrophysical Journal, 812, 18

Walt, S. v. d., Colbert, S. C., & Varoquaux, G. 2011, Computing in Science & Engineering, 13, 22

Yu, L., Winn, J. N., Gillon, M., et al. 2015, The Astrophysical Journal, 812, 48

Zasowski, G., Cohen, R. E., Chojnowski, S. D., et al. 2017, The Astronomical Journal, 154, 198

Ziegler, C., Law, N. M., Baranec, C., et al. 2018, arXiv:1806.10142 [astro-ph], arXiv: 1806.10142